Electrochemical and Solid-State Letters, **9** (9) A430-A434 (2006)
1099-0062/2006/9(9)/A430/5/$20.00 © The Electrochemical Society

X-Ray Absorption Spectroscopy Studies of Water Activation on an Rh_xS_y Electrocatalyst for Oxygen Reduction Reaction Applications

J. M. Ziegelbauer,[a,*] D. Gatewood,[b,*] A. F. Gullá,[c] D. E. Ramaker,[b,] and S. Mukerjee[a,**,z]**

[a]*Department of Chemistry and Chemical Biology, Northeastern University, Boston, Massachusetts 02115, USA*
[b]*Department of Chemistry, The George Washington University, Washington, D.C. 20052, USA*
[c]*PEMEAS Fuel Cell Technologies, E-TEK Division, Somerset, New Jersey 08873, USA*

The prototype chalcogenide electrocatalyst Rh_xS_y was probed in situ via a synchrotron-based X-ray absorption near-edge structure (XANES) technique to elucidate specific sites and modes of water activation during oxygen reduction reaction. X-ray diffraction revealed a mixture of phases (Rh_2S_3, Rh_3S_4, and $Rh_{17}S_{15}$). Theoretically generated XANES on a variety of geometries of O(H) adsorption on the predominant Rh_3S_4 phase were compared to the experimental data. We show for the first time that the electrocatalyst first adsorbs O(H) in a onefold configuration at lower potentials and *n*-fold at potentials greater than 0.80 V. This expectedly has important consequences for oxygen reduction reaction on alternative chalcogenide materials.
 [DOI: 10.1149/1.2218304]

Manuscript submitted March 2, 2006; revised manuscript received May 25, 2006. Available electronically June 28, 2006.

The current state-of-the-art materials for low- and medium-temperature fuel cell cathodes are platinum or platinum-transition metal alloys. Platinum has a high activity for oxygen reduction reaction (ORR), ($i_0 \approx 10^{-5}$ mA cm^{-2}) and tends predominantly towards the 4_e^- oxygen reduction process. Unfortunately, platinum is extremely expensive, low in abundance, and easily poisoned. Even small amounts of contaminants severely depolarize platinum cathodes; this is a major issue in the context of direct methanol fuel cells (DMFCs). Methanol crossover through the proton exchange membrane and the resulting depolarization of a platinum-based catalyst causes overpotential losses of the order of approximately 300 mV vs reference hydrogen electrode (RHE). It is also important to note that in the case of electrolyzers such as those used for chlorine generation, cathodic oxygen reduction is preferred from both energy-saving and safety perspectives.[1,2] Here, Pt-based electrocatalysts are not applicable due to their inherently higher solubility and susceptibility to poisoning in chlorine-saturated HCl.[1,2]

As a result of these economic and technical issues, many groups are currently searching for new materials to replace platinum in these applications, such as transition metal chalcogenide clusters.[3,4] A wealth of research has generally pointed to pseudobinary $M_xRu_ySe_z$ clusters (where M = transition metal) as exhibiting the best performance (i_0:Ru_xSe_y/C = 2.22 $\times$ 10^{-5}, 0.5 M H_2SO_4).[5,6] While these clusters are active towards ORR and exhibit a high degree of methanol tolerance, the pertinent structure/property relationships are still unclear.[7]

One of the important variables to full 4_e^- ORR is the water activation pathway. In the case of Pt-based electrolcatalysts, the adsorption of OH (as well as halide ions) on the electrocatalyst surface acts as a surface poison towards O_2 adsorption.[8] These effects on Pt and Pt-alloy systems have been extensively studied.[9,10] A recent study examined the effects of OH adsorption on Pt and Pt alloys by varying the concentration of water in a trifluoromethane sulfonic acid (TFMSA) electrolyte (where 6 M corresponds to a 4:1 mol % H_2O/SO_3^- ratio).[9] The ~60 mV/dec Tafel slope observed at low overpotentials was related to OH(ads) coverage, and the higher performance exhibited by the Pt alloys was attributed to two effects. Either the alloyed transition metal takes the brunt of OH adsorption in cases where homogeneous alloy formation results in enough transition metal atoms on the surface, or a deactivation of the Pt surface (involving an increased partial valence of Pt) shifts the onset of OH formation to higher potentials.[9,11,12]

These conclusions were bolstered by ab initio calculations and experimentally determined apparent activation energies (E_a^*) for ORR on Pt and Pt-alloy electrocatalysts.[13,14] In both cases, a downward trend of the E_a values were observed in respect to increasing overpotential and indicated that differences in oxide layer formation on these systems influence the preexponential term in the Arrhenius equation.[9] This was related to a surface coverage expression derived by Paulus and Marković with the initial electron transfer as the rate-determining step.[15,16] Successive calculations by Anderson et al. lead to the conclusion that reduction of the H_2O_2 intermediate possessed the highest activation energy and is closely followed by the first electron reduction of adsorbed oxygen.[17] The lowest activation energies corresponded to the formation of ·OOH(ads) and ·OH(ads).[13]

Another recent technique that has assisted in elucidating ORR on Pt and Pt alloys is the "delta mu" ($\Delta\mu$) analysis of X-ray absorption spectra measured in situ under electrochemical control via synchrotron radiation to study the water activation pathway.[18,19] The $\Delta\mu$ technique entails a specific normalization of the absorption data[18,20-22] and allows for the observation of adsorbates on the electrocatalyst surface, including the specific site symmetry, as a function of potential.[10,23] Subsequent modeling of Pt and Pt-alloy spectra showed that OH adsorbs in an atop configuration at low potentials proceeding to bridge-bonded (twofold) O geometry at ~0.9 V, and finally three- and fourfold O [e.g., face-centered cubic (fcc) and hexagonal close-packed (hcp)-coordinated O] at $E > 0.95$ V.[10,23,24] Place exchange, initially proposed by Wroblowa et al.[25] appeared at a potential of 1.05 V.[10] Historically, this was the first time that the place-exchange mechanism on a Pt electrocatalyst was spectroscopically observed under in situ operating conditions. Prior density functional theory (DFT) calculations to determine OH and O binding preferences on identical Pt_6 clusters agreed well with the results of the $\Delta\mu$ analysis.[26,27]

Here we have studied a mixed-phase 30 wt % Rh_xS_y/VXC72 electrocatalyst by both rotating disk electrode (RDE) and in situ X-ray absorption spectroscopy (XAS). Rh_xS_y shows significant activity in acid electrolytes and maintains a rigorous selectivity towards ORR in the presence of large concentrations of methanol.[5,7,28] Recent patent literature has promoted Rh_xS_y as a promising candidate in the harsh environments of chlor-alkali production.[29-33] Not only is this material commercially available from E-TEK, Inc. (Somerset, NJ, a division of PEMEAS Fuel Cell Technologies),[31,32]

* Electrochemical Society Student Member.
** Electrochemical Society Active Member.
z E-mail: s.mukerjee@neu.edu

but, in contrast to previous reports on materials synthesized according to the nonaqueous route,[34] the material from E-TEK possesses long-range order and is therefore ideally suited for the modeling necessary for $\Delta\mu$ interpretation. Through examination of the activation energies and water activation via the $\Delta\mu$ technique we not only show the correlation between surface coverage (water activation) and the specific ORR kinetics on a chalcogenide electrocatalyst but also validate the $\Delta\mu$ analysis technique for structurally complex mixed-phase chalcogenide ORR electrocatalysts.

Experimental

Electrochemical characterization.— RDE studies were conducted according to procedures described in detail elsewhere.[9] Briefly, inks of 30 wt % Rh_xS_y/VXC72 (E-TEK) were prepared by combining the catalyst, deionized water (18.2 MΩ, Millipore MilliQ system), 2-propanol (HPLC grade, Aldrich), and 5 wt % Nafion solution (Aldrich). The ink was then cast on a 6 mm diameter polished glassy carbon (gc) rotating disk electrode (Pine Instrument Co.) to give a final metal loading of 14 μg metal with a Nafion catalyst ratio of 1:50 (weight). Activation energies for the material were determined by analyzing RDE data obtained at 100, 400, 625, 900, 1225, and 1600 rpm at 20, 30, 40, 50, and 60°C in O_2-saturated 0.5 M H_2SO_4 (HPLC Grade, Aldrich).[9,15,35,36] All data was collected with an Autolab potentiostat (model PGSTAT30, Ecochemie-Brinkmann) with a sealed RHE, filled with same electrolyte as the bulk cell as the reference electrode and a Pt mesh serving as the counter electrode.

In situ XAS data collection and analysis.— All experiments were performed at room temperature in an inert electrochemical cell (based on a previously reported design)[37] to capture the essence of water activation sans interference. The cells consisted of a 30 wt % Rh_xS_y/VXC72 working electrode, 20 wt % Au/VXC72 (E-TEK) counter electrode, and a RHE in 1 M TFMSA (3M Corporation) electrolyte with a Nafion 112 membrane (DuPont) acting as a separator. TFMSA was utilized for its low anion adsorption effects[10] and was extensively purified according to the methods described elsewhere.[38-40] The inks were hand-painted onto commercially available ELAT V2 (E-TEK) gas diffusion electrodes (95:5 30 wt % catalyst/Nafion binder by mass) and cut into 5.0 cm squares. The total geometric metal loadings of the anode and cathode were 0.7–1.5 mg metal cm^{-2} and were chosen to be approximately 10% of the loading to give a transmission XAS absorption cross section of ~1. In all cases, 0.35 mm Au wires (99.995%, Alfa-Aesar) were used as the current collectors.

Following an activation step (0.02 to 1.2 V vs RHE at 20 mV s^{-1}), full Rh K edge (23220 eV) extended X-ray absorption fine structure (EXAFS) scans (−250 eV to 18 k) were collected at different potentials by cycling the cell to the respective anodic potential and holding potentiostatically during the absorption measurements. These measurements were collected in fluorescence mode via a 13-element fluorescence detector at beamline X18-B (National Synchrotron Light Source, Brookhaven National Labs, Upton, NY). During all the measurements transmission data was collected in conjunction with a thin Rh foil. For alignment, background subtraction, and normalization of the XAS data, the IFEFFIT suite (version 1.2.4, IFEFFIT Copyright 1997-2002, Matthew Newville, http://cars9.uchicago.edu/ifeffit/) was utilized.[41]

The theory and normalization processes for the $\Delta\mu$ analysis are described in detail elsewhere.[18,20,21,42] Briefly, the collected spectra were aligned by using the signals from the reference foil in order to preserve any shifts in the absorption edge arising from oxidation of the Rh. The aligned spectra were then carefully normalized in a previously described manner.[22] Difference spectra were generated according to the relationship

$$\Delta\mu = \mu(V) - \mu(0.40\ V) \quad [1]$$

where the signal at 0.40 V is considered the cleanest (e.g., double layer) region free of adsorbed H, O(H), and $CF_3SO_3^-$ anions. Due to the mixed-phase character of the Rh_xS_y catalyst, it is impossible to say that the 0.40 V signal represents the true adsorbate-free region. However, trials involving baseline subtraction of other potentials (0.30 and 0.50 V) did not yield a clean and systematic spectrum. For the $\Delta\mu$ signals at 0.50 and 0.60 V a correction to account for both charging effects of the electrode and the Rh lifetime core width was performed.[10,43] Fitting of the acquired spectra was accomplished by first constructing 3D models of the Rh_3S_4 (Rh_6S_x) clusters with various adsorbed O(H) species in differing locations and geometries and generating XANES spectra with FEFF 8.0.[10,23,24] Interpretation of the results was accomplished by comparison of the experimental and theoretical $\Delta\mu = \mu(Rh_6O_x) - \mu(Rh_6)$ spectra.

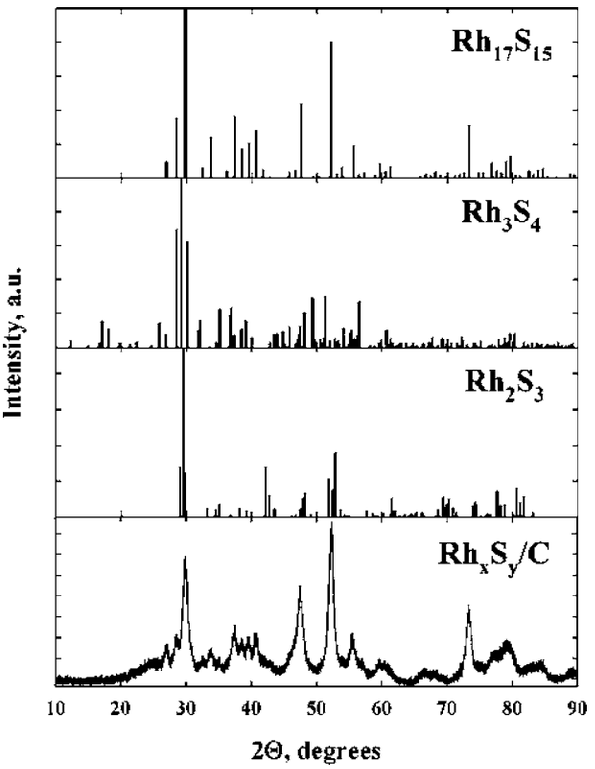

Figure 1. Cu Kα X-ray powder diffractogram for the 30 wt % Rh_xS_y/VXC72 electrocatalyst (E-TEK). The patterns are indicative of a balanced-phase mixture of Rh_2S_3, Rh_3S_4, and $Rh_{17}S_{15}$ phases with an insignificant amount of fcc Rh metal present. The single-phase diffractograms were reproduced from Ref. 48, 50, and 51.

Results and Discussion

X-ray diffraction (XRD).— Analysis of the powder XRD spectrum for the 30 wt% Rh_xS_y/VXC72 electrocatalyst (Fig. 1) poses considerable complexities. Since the first systematic XRD investigations of rhodium–sulfur chalcogen systems were reported during the 1930s, a considerable number of complexes have been recognized.[44-47] Geller undertook single-crystal studies an investigation of a single crystal of $Rh_{17}S_{15}$ (and its Pd-based analogue: $Pd_{17}Se_{15}$) in 1962.[48,49] While the indexing could be accomplished with a variety of space groups, the cubic $Pm\bar{3}m$ symmetry gave the lowest standard errors. The result was a material consisting of alternating Rh-rich and S-rich layers. Another phase, orthorhombic *Pbcn* Rh_2S_3, was investigated in tandem with Ir- and Se-based analogues in the early 1960s.[50] Rh_2S_3 was found to consist of alternating RhS_6 octahedra with an average Rh–Rh bond length of 3.208 Å. As the average Rh–Rh distance in metallic Rh is 2.69 Å, the possibility of direct Rh–Rh bonds, and hence any metallic character, was discounted. The final morphology of interest is the monoclinic

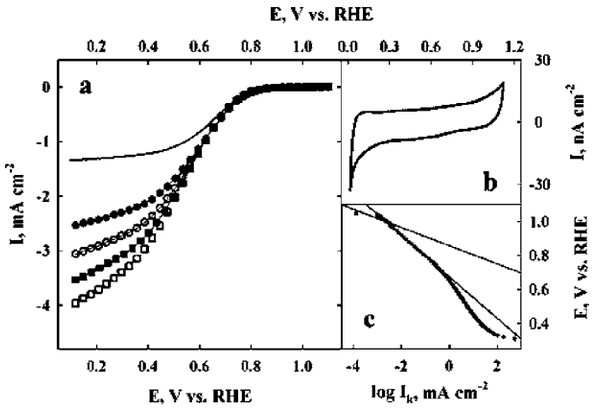

Figure 2. ORR curves for 30 wt % Rh_xS_y/VXC72 (E-TEK) in room temperature (293 K) $O_{2(g)}$-saturated 0.5 M H_2SO_4 at 10 mV s^{-1}. (a) From top to bottom: 100, 400, 625, 900, and 1225 rpm, (b) cyclic voltammogram of the same electrocatalyst in $Ar_{(g)}$-saturated 0.5 M H_2SO_4 at 20 mV s^{-1} (T = 293 K), and (c) mass-transfer-corrected Tafel plot of the data collected at 900 rpm.

$C_{2/m}$ Rh_3S_4 phase.[51] The Rh_3S_4 material resides between the nonmetallic Rh_2S_3 and metallic $Rh_{17}S_{15}$ phases and exhibits properties akin to both of its brethren. RhS_6 octahedra (essentially Rh_2S_3) serve as the backbone in the Rh_3S_4 phase and anchor metallic Rh_6 eaves. In addition, Beck and Hilbert's studies confirm the mixed–phase character of these materials.[51]

As a result of the synthetic methodology,[31] Rh_xS_y is considered to be a balanced-phase mixture of Rh_2S_3/Rh_3S_4/$Rh_{17}S_{15}$. In Fig. 1, the 4-peak cluster at 37–40.5° is indicative of the balanced phase (and the presence of $Rh_{17}S_{15}$), while the intensities of the 3 large peaks slightly below 30° points to the Rh_2S_3 phase [29.1° (002), 29.6° (211), 29.8° (020)], and the Rh_3S_4 phase is indicated by the (130) and (131) peaks appearing at 26.6° and 29.3°, respectively, in the Rh_xS_y/VXC72 spectrum. In addition, the (311) facet of fcc rhodium metal is observed at 47.3°, but the relative intensity indicates only a small amount is present.

Rotating disk studies.— The results for the room temperature RDE studies of the 30 wt % Rh_xS_y/VXC72 is shown in Fig. 2. It is immediately apparent that the voltammogram (Fig. 2b) is relatively featureless. However, a close examination reveals a slight cathodic peak extending from 0.7 to 0.3 V. The reasons behind this feature are not clearly defined at the moment, for, as described above, the Rh_xS_y is fully hetereogeneous. Possible explanations involve Rh ion reduction,[52] oxo-monolayer or oxygen reduction, and possibly bisulfate anion adsorption.[53] A more complete description of these features regarding the synthesis and electrochemical characterizations of the Rh_xS_y single phases will be reported at a later date.[54]

While the ORR curves exhibit a large kinetic fingerprint (Fig. 2a), the lack of a well-defined limiting current region makes a rigorous kinetic analysis difficult. Nonetheless a mass-transfer-corrected Tafel plot (900 rpm, Fig. 2c) was constructed by utilizing the region where the slope of the current became constant. Analysis revealed two specific regions with slopes of −58 and −122 mV dec^{-1} over a 1.04–0.75 V region. These features are strikingly similar to those observed for Pt-based electrocatalysts. Further, Rh_xS_y possesses a fairly high onset potential for ORR as determined by a first derivative transform of the reduction waves (vs +1.1 V for Pt in similar O_2-saturated conditions). When compared to the more common Ru-based sulfides and selenides (which suffer irreversible Ru and Se oxidation at potentials greater than ~0.85 V),[36,55] Rh_xS_y offers substantial performance gains, especially when considering the inherent methanol tolerance of chalcogenide electrocatalysts.[5,28,55]

Table I. Activation energies as a function of potential. The 30 wt% Rh_xS_y/VXC72 moiety was collected in 0.5 M H_2SO_4. The 20 wt % Pt-based catalysts, shown for comparison, are from Ref. 9 and 13.

Electrocatalyst	E_a^* (0.85 V) (kJ mol^{-1})	E_a^* (0.80 V) (kJ mol^{-1})	E_a^* (0.75 V) (kJ mol^{-1})	E_a^* (0.70 V) (kJ mol^{-1})
Rh_xS_y/C	22.65 ± 2.02	21.81 ± 1.90	19.13 ± 2.22	17.33 ± 1.87
Pt/C	27.84 ± 2.04	26.87 ± 2.0	22.13 ± 1.7	19.12 ± 1.8
PtCo/C	27.86 ± 0.23	25.18 ± 0.78	22.33 ± 0.33	19.02 ± 0.78

Table I presents a comparison of the activation energies for the 30 wt % Rh_xS_y/VXC72 electrocatalyst compared to previously reported 20 wt % Pt and Pt alloys[9] as determined by a modified Arrhenius equation[15,35]

$$\left(\frac{\partial \log(i)}{\partial (1/T)}\right)_E = \frac{E_a^*}{2.3R} \qquad [2]$$

where i is the current, T is temperature (in Kelvin), E is the constant potential term, E_a^* is the activation energy (kJ mol^{-1}), and R is the gas constant. An overall trend of decreasing activation energies in respect to increasing overpotential is evident for all of the catalysts. Comparison with prior results for Pt and Pt-based alloys,[13] coupled with the inherent similarity of the activation energy trends for the Rh_xS_y moiety, suggests that the mixed-phase 30 wt % Rh_xS_y/VXC72 electrocatalyst not only proceeds through a similar formation of ·OOH(ads) species at lower potentials but may accomplish ORR on geometrically similar active sites. Further analysis of the Rh_xS_y results, including qualitative estimations of the relative densities of active sites in relation to potential, would require similar time-consuming DFT calculations.[13] However, a spectroscopic ($\Delta\mu$) analysis of water activation as reported for Pt-based electrocatalysts[10,24] was readily accomplished in a comparatively short amount of time. If the assumptions gleaned from the activation energy studies are correct, then the corresponding $\Delta\mu$ analysis should reveal a water activation pathway similar to that reported for the Pt and Pt-alloy electrocatalyst systems.[10]

In situ XAS.— The in situ XANES spectrum for the 30 wt % Rh_xS_y/VXC72 electrocatalyst collected at different potentials is presented in Fig. 3a. From analysis of the absorption edge energy (Rh K edge = 23220 eV), it would appear that the Rh present in the sample is fully reduced. Comparison with the Rh reference foil (grey line), however, clearly shows that while the Rh in the material may have an adsorption edge indicating an average oxidation state of 0, it is not a fully reduced Rh metal. While the line shapes and

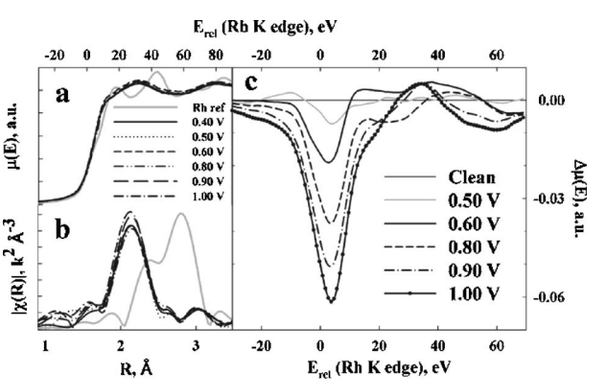

Figure 3. Rh K edge (23220 eV) XAS spectra for 30 wt % Rh_xS_y/VXC72 (E-TEK) in 1 M TFMSA at different anodic potentials: (a) XANES, (b) forward Fourier transform (phase corrected, k^2 weighted, ΔR = 0.02 Å), and (c) $\Delta\mu = \mu(V) - \mu(0.40\ V)$ spectrum.

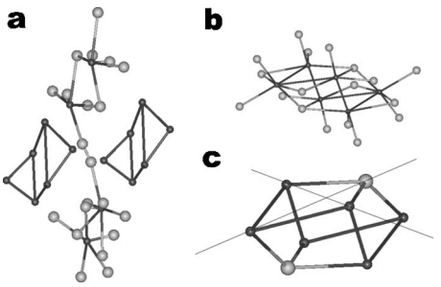

Figure 4. 3D representations of the monoclinic $C_{2/m}$ Rh_3S_4 moiety (Ref. 50) used for fitting the $\Delta\mu$ spectra. The Rh atoms are the smaller, darker circles, while the sulfur atoms are the large diameter light-colored orbs. (a) Full unit cell of Rh_3S_4, (b) a single, fully sulfided Rh_6 eave (octahedral cluster), and (c) a stripped version of the Rh_6 cluster used in the calculations with the "equatorial" geometry shown as a solid line passing through two Rh atoms and the "axial" geometry as the line that passes through an Rh and S atom.

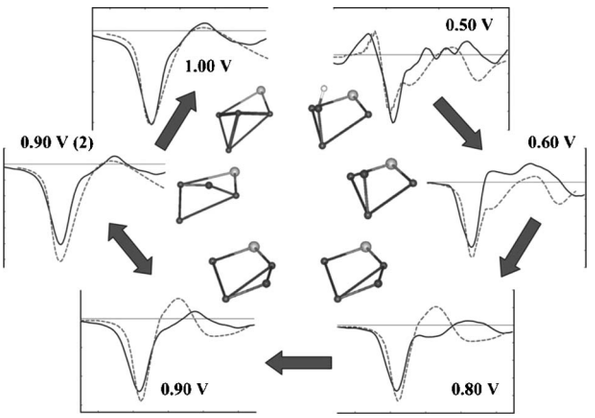

Figure 5. Theoretical FEFF 8.0 (dashed) fits and (solid) experimentally derived $\Delta\mu$ curves for the 30 wt % Rh_xS_y/VXC72 (E-TEK) electrocatalyst in 1 M TFMSA shown with the corresponding oxygenated models used to generate the fits.

amplitudes past the edge correspond closely to those observed for an oxidized Rh metal, the amplitude shifts are too small to directly expound upon the extent of oxidation.

In light of the limitations of the X-ray absorption near-edge structure (XANES) analysis, a forward Fourier transform (k^2 weighted) of the corresponding EXAFS data was performed (Fig. 3b). The peak amplitudes in these transforms correspond to quantitative shifts in both the coordination number and Debye–Waller factor of the studied element and are plotted against interatomic distance (±0.02 Å). Like the XANES spectrum (Fig. 3a) the Fourier transformed (FT) spectrum shows clear differences between the Rh_xS_y electrocatalyst and Rh metal. The strong Rh–Rh interactions present in the Rh reference foil (R = 2.69 Å) are almost completely damped out in the spectra for the Rh_xS_y moiety. Based on the XRD data, it is not surprising to find that the catalyst is primarily composed of materials that are dominated by Rh–S and Rh–O interactions ranging from 2.1 to 2.4 Å (ΔR = 0.02 Å). Most important, the Rh–O peak amplitudes at ~2.1 Å undergo systematic increases with respect to an increase in potential. Unfortunately, EXAFS is a bulk-averaging technique and proper separation and identification of the Rh–O interactions of the three balanced phases is too complicated to be considered reliable.

The corresponding $\Delta\mu = \mu(V) - \mu(0.40\ V)$ spectrum of the 30 wt % Rh_xS_y/VXC72 catalyst is shown in Fig. 3c. Compared to the XANES and EXAFS spectra in Fig. 3a and b, clear and systematic differences are occurring with respect to potential. The line shapes in the potential regions 0.50–0.60 V vs RHE show clear shoulders before and after the primary minima and a clear change in the post-peak shoulder shape between 0.80 and 0.90 V, and an overall increase in peak amplitude is observed from low (0.50 V) to high (1.00 V) potentials. For the fitting of the Rh_xS_y $\Delta\mu$ spectrum, Rh_3S_4 (Fig. 4) was chosen. As previously described, this material consists of a heavily sulfided RhS_6 backbone with the two metallic octahedral Rh_6 eaves on either side. Based on the morphology of the material and chemical intuition, it is apparent that charge transfer occurs predominately at these metallic eaves. A comparison of numerous fits to the experimental data, and the corresponding models, is presented in Fig. 5.

At the lowest measured potential, 0.50 V, only an atop (onefold) OH was able to reproduce both the low intensity of the first peak minimum in addition to the preceding positive intensity shoulder. At 0.60 V adsorbed OH would not reproduce the shoulders before and after the main minimum peak. Instead it was found that only an adsorbed onefold O would fit the spectrum. By 0.80 V onefold O species have been replaced by twofold O in the axial position, suggesting that replacement of a sulfur atom occurs between 0.60 and 0.80 V. As with 0.80 V, only twofold O would give an adequate fit at 0.90 V. Interestingly, the twofold O is a mixture of both the axial and equatorial positions. At 1.00 V, the highest potential at which data was collected, the spectrum is clearly dominated by *n*-fold O. There is no evidence of subsurface O, or place exchange of the metal atoms, as reported for the Pt/C electrocatalysts.[10]

Based on the similarity of the previously discussed activation energies to Pt/C systems (Table I), it would not be surprising to see a correlation between the two systems in respect to the water activation pathway. As expected, the Rh_xS_y is primarily covered with onefold O(H) at potentials from 0.50–0.60 V. From 0.80 to 1.00 V the surface is predominantly covered by two- and *n*-fold O, suggesting that water of hydration is not affecting the catalyst. When compared to the reported Pt and Pt-alloy systems,[9,10,24] the Rh_3S_4 phase of the 30 wt % Rh_xS_y/VXC72 electrocatalyst behaves in a remarkably similar manner.

Conclusion

Application of the $\Delta\mu$ technique to in situ XAS data collected under real electrochemical conditions coupled with activation energy measurements has allowed, for the first time, the direct observation of the water activation on a heterogeneous 30 wt% Rh_xS_y/VXC72 (E-TEK) chalcogenide electrocatalyst via the modeling of the Rh_3S_4 phase. Not only is a clear delineation between one- and *n*-fold adsorbed O(H) species observable, but the specific site symmetry of adsorption on the catalyst has been clarified. Akin to Pt/C electrocatalysts, the surface of Rh_3S_4 is dominated by onefold O(H) species at low potentials. Beginning at 0.80 V, a successive parade of twofold to *n*-fold adsorbed O dominates on the surface. Similarities to the activation energies for ORR of Pt/C systems nonwithstanding, the nearly identical nature of the water activation process is remarkable.

The ramifications of this examination are significant. First, the $\Delta\mu$ technique has been previously successfully applied to homogeneous Pt and Pt-alloy electrocatalysts. Compared to a mixed-phase chalcogenide material, however, those prior investigations were considerably easier to perform. Here the $\Delta\mu$ analysis was proven not only to function in a mixed-phase environment but also supplied the chemical information necessary to discern the active sites for water activation in respect to potential. Indeed, considering the considerable amount of work performed over the past decades to understand the kinetics of ORR on Pt-based electrocatalysts, the time scale of this investigation on a chalcogenide electrocatalyst is significantly brief. It is anticipated that future examinations on the phases present in the 30 wt % Rh_xS_y/VXC72 electrocatalyst will convey similarly detailed information.

Acknowledgments

The authors are grateful to the E-TEK Division of PEMEAS Fuel Cell Technologies, in particular to Robert J. Allen, for their financial and material assistance. Also, the authors are thankful for the use of the X-18B beamline at the National Synchrotron Light Source, Brookhaven National Laboratory, which is supported by the U.S. Department of Energy, Office of Science, Office of Basic Energy Sciences, under contract no. DE-AC02-98CH10886.

Northeastern University assisted in meeting the publication costs of this article.

References

1. F. Gestermann, *Oxygen Depolarized Cathodes in the Chlor Alkali Electrolysis - on the Way to Industrial Application*, p. 186, Electrolysis in the Chemical Industry, Clearwater Beach, FL (1998).
2. F. Gestermann and A. Ottaviani, *Mod. Chlor-Alkali Tech.*, **8**, 49 (2001).
3. N. A. Vante and H. Tributsch, *Nature (London)*, **323**, 431 (1986).
4. N. A. Vante, W. Jaegermann, H. Tributsch, W. Hoenle, and K. Yvon, *J. Am. Chem. Soc.*, **109**, 3251 (1987).
5. A. K. Shukla and R. K. Raman, *Annu. Rev. Mater. Res.*, **33**, 155 (2003).
6. R. G. González-Huerta, J. A. Chávez-Carvayar, and O. Solorza-Feria, *J. Power Sources*, **153**, 11 (2006).
7. N. Alonso-Vante, in *Catalysis and Electrocatalysis at Nanoparticle Surfaces*, A. Wieckowski, E. R. Savinova, and C. G. Vayenas, Editors, p. 931, Marcel Dekker, New York (2003).
8. R. R. Adzic, in *Electrocatalysis*, J. Lipkowski and P. N. Ross, Editors, p. 197, Wiley-VCH, New York (1998).
9. V. S. Murthi, R. C. Urian, and S. Mukerjee, *J. Phys. Chem. B*, **108**, 11011 (2004).
10. M. Teliska, W. E. O'Grady, and D. E. Ramaker, *J. Phys. Chem. B*, **109**, 8076 (2005).
11. S. Mukerjee and R. C. Urian, *Electrochim. Acta*, **47**, 3219 (2002).
12. S. Mukerjee, R. C. Urian, C. K. Witham, T. I. Valdez, and S. R. Narayanan, in *Direct Methanol Fuel Cells*, S. R. Narayanan, S. Gottesfeld, and T. Zawodzinski, Editors, PV 2001-4, p. 136, The Electrochemical Society Proceedings Series, Pennington, NJ (2001).
13. A. B. Anderson, J. Roques, S. Mukerjee, V. S. Murthi, N. M. Markovic, and V. Stamenkovic, *J. Phys. Chem. B*, **109**, 1198 (2005).
14. A. B. Anderson, N. M. Neshev, R. A. Sidik, and P. Shiller, *Electrochim. Acta*, **47**, 2999 (2002).
15. U. A. Paulus, A. Wokaun, G. G. Scherer, T. J. Schmidt, V. Stamenkovic, V. Radmilovic, N. M. Markovic, and P. N. Ross, *J. Phys. Chem. B*, **106**, 4181 (2002).
16. N. M. Marković, H. A. Gasteiger, B. N. Grgur, and P. N. Ross, *J. Electroanal. Chem.*, **467**, 157 (1999).
17. A. B. Anderson and T. V. Albu, *J. Electrochem. Soc.*, **147**, 4229 (2000).
18. D. E. Ramaker, B. L. Mojet, D. C. Koningsberger, and W. E. O'Grady, *J. Phys.: Condens. Matter*, **10**, 8753 (1998).
19. B. A. Bunker and E. A. Stern, *Phys. Rev. B*, **27**, 1017 (1983).
20. D. C. Koningsberger, B. L. Mojet, J. T. Miller, and D. E. Ramaker, *J. Synchrotron Radiat.*, **6**, 135 (1999).
21. D. E. Ramaker, B. L. Mojet, J. T. Miller, and D. C. Koningsberger, *Top. Catal.*, **10**, 157 (2000).
22. G. E. van Dorssen, D. C. Koningsberger, and D. E. Ramaker, *J. Phys.: Condens. Matter*, **14**, 13529 (2002).
23. M. Teliska, W. E. O'Grady, and D. E. Ramaker, *J. Phys. Chem. B*, **108**, 2333 (2004).
24. M. Teliska, V. S. Murthi, S. Mukerjee, and D. E. Ramaker, *J. Electrochem. Soc.*, **152**, A1259 (2005).
25. J. O. M. Bockris, H. Wroblowa, and V. Brusic, *J. Phys. Chem.*, **75**, 2823 (1971).
26. D. E. Ramaker, M. Teliska, Y. Zhang, A. Yu, and D. C. Koningsberger, *Phys. Chem. Chem. Phys.*, **5**, 4492 (2003).
27. E. Janin, H. von Schenck, M. Göthelid, and U. O. Karlsson, *Phys. Rev. B*, **61**, 13144 (2000).
28. R. W. Reeve, P. A. Christensen, A. J. Dickinson, A. Hamnett, and K. Scott, *Electrochim. Acta*, **45**, 4237 (2000).
29. R. J. Allen, J. R. Giallombardo, D. Czerwiec, E. S. De Castro, and K. Shaikh, U.S. Pat. 6,149,782 (2000).
30. R. J. Allen, J. R. Giallombardo, D. Czerwiec, E. S. De Castro, K. Shaikh, F. Gestermann, H.-D. Pinter, and G. Speer, U.S. Pat. 6,402,930 (2002).
31. A. F. Gullá and R. J. Allen, U.S. Pat. 6967185B2 (2005).
32. A. F. Gullá, R. J. Allen, and E. S. De Castro, U.S. Pat. Appl. 2004/024142412A1 (2004).
33. A. F. Gullá, J. M. Ziegelbauer, R. J. Allen, and S. Mukerjee, In preparation.
34. O. Solorza-Feria, K. Ellmer, M. Giersig, and N. Alonso-Vante, *Electrochim. Acta*, **39**, 1647 (1994).
35. U. A. Paulus, T. J. Schmidt, H. A. Gasteiger, and R. J. Behm, *J. Electroanal. Chem.*, **495**, 134 (2001).
36. T. J. Schmidt, U. A. Paulus, H. A. Gasteiger, N. Alonso-Vante, and R. J. Behm, *J. Electrochem. Soc.*, **147**, 2620 (2000).
37. J. McBreen, W. E. O'Grady, K. I. Pandya, R. W. Hoffman, and D. E. Sayers, *Langmuir*, **3**, 428 (1987).
38. M. A. Enayetullah, T. D. DeVilbiss, and J. O. M. Bockris, *J. Electrochem. Soc.*, **136**, 3369 (1989).
39. M. A. Enayetullah, Ph.D. Thesis, Case Western Reserve University, Cleveland, OH (1986).
40. P. N. Ross and P. C. Andricacos, *J. Electroanal. Chem. Interfacial Electrochem.*, **154**, 205 (1983).
41. M. Newville, *J. Synchrotron Radiat.*, **8**, 322 (2001).
42. D. C. Koningsberger, B. L. Mojet, G. E. van Dorssen, and D. E. Ramaker, *Top. Catal.*, **10**, 143 (2000).
43. M. H. Chen, B. Crasemann, and H. Mark, *Phys. Rev. A*, **24**, 177 (1981).
44. R. Juza, O. Hülsmann, K. Meisel, and W. Biltz, *Z. Anorg. Allg. Chem.*, **225**, 369 (1935).
45. W. Biltz, *Z. Anorg. Allg. Chem.*, **233**, 282 (1937).
46. A. Dey and V. K. Jain, *Platinum Met. Rev.*, **48**, 16 (2004).
47. I. Dance and K. Fisher, in *Progress in Inorganic Chemistry*, K. D. Karlin, Editor, p. 637, John Wiley & Sons, Inc., New York (1994).
48. S. Geller, *Acta Crystallogr.*, **15**, 1198 (1962).
49. S. Geller, *Acta Crystallogr.*, **15**, 713 (1962).
50. E. Parthe, D. K. Hohnke, and F. Hulliger, *Acta Crystallogr.*, **23**, 832 (1967).
51. J. Beck and T. Hilbert, *Z. Anorg. Allg. Chem.*, **626**, 72 (2000).
52. M. Pourbaix, *Atlas of Electrochemical Equilibria in Aqueous Solutions*, p. 350, Pergamon Press, London (1966).
53. Y. Shingaya and M. Ito, *J. Electroanal. Chem.*, **467**, 299 (1999).
54. J. M. Ziegelbauer, A. F. Gullá, and S. Mukerjee, In preparation.
55. H. Schulenburg, M. Hilgendorff, I. Dorbandt, J. Radnick, P. Bogdanoff, S. Fiechter, M. Bron, and H. Tributsch, *J. Power Sources*, **155**, 147 (2005).